coatings

MDPI

Article

Experimental Study on the Mechanical Properties of Basalt Fiber Geogrids Reinforced with Cement-Stabilized Macadam

Yu Zhu [1], Yuan He [2], Xiaodong Yuan [1], Jiangping Gao [2,*] and Zhi Wang [2]

[1] Yanchong Branch, Hebei Expressway Group Co., Ltd., Zhangjiakou 075000, China
[2] Key Laboratory of Highway Engineering in Special Areas, Chang'an University, Ministry of Education, Xi'an 710064, China
* Correspondence: jiangpinggao@chd.edu.cn

Abstract: Cement-stabilized crushed stone is widely used in the construction of high-grade highways because of its good durability and stability. However, cement-stabilized gravel is also easily affected by temperature and humidity, resulting in a reduction in the overall strength and durability of asphalt pavement. In response to this problem, in this study, we lay a single layer of a basalt fiber geogrids in a cement-stabilized gravel base of a test section of the Yan-Chong Expressway. The bonding and friction forces formed between the basalt fiber geogrids and the base as well as the mechanical bite force, play an anti-cracking role. We conducted a comparative experimental study on the mechanical properties of basalt fiber geogrids reinforced or not reinforced with cement-stabilized gravel specimens of different ages. The results showed that (1) the unconfined compressive strength of cement-stabilized gravel was slightly reduced; (2) the splitting strength was somewhat improved; (3) the compressive elastic modulus was slightly reduced; (4) the flexural and tensile strengths were significantly increased. An improvement in the crack resistance in semi-rigid base materials can improve the service life of high-grade asphalt pavements.

Keywords: cement-stabilized macadam; basalt fiber geogrid; mechanical property; curing age

Citation: Zhu, Y.; He, Y.; Yuan, X.; Gao, J.; Wang, Z. Experimental Study on the Mechanical Properties of Basalt Fiber Geogrids Reinforced with Cement-Stabilized Macadam. *Coatings* **2024**, *14*, 1349. https://doi.org/10.3390/coatings14111349

Academic Editor: Andrea Nobili

Received: 9 August 2024
Revised: 4 October 2024
Accepted: 8 October 2024
Published: 23 October 2024

1. Introduction

As the most commonly used base material for advanced pavement, cement- stabilized macadam is characterized by a high strength (which increases with curing age), good plate and deflection properties, and a strong load diffusion abilities. As such, it is widely used as the base of highway pavements. However, reflection cracks in asphalt pavement caused by dry shrinkage and temperature shrinkage are a common problem in pavement structures [1–3]. Therefore, it is of great significance to reduce crack generation in asphalt pavements with a semi-rigid base.

In view of the above problem, scholars have proposed incorporating fiber into cement-stabilized materials to suppress cracking of the base. Some scholars [4–7] have shown that adding steel, polypropylene, and basalt fibers can change the mechanical strength and toughness of cement-based materials. Basalt fiber has the advantages of a high tensile strength, good mechanical properties, and resistances to high temperature, ultraviolet radiation, acidity, alkalinity, salt, and aging, and does not require waste water, gas, or other industrial wastes throughout its entire production process. In addition, basalt ore is quite abundant, ensuring a relatively low raw material cost and a long product life. The price of basalt fiber is also 1/8 to 1/6 that of carbon fiber, which is a new type of environmentally friendly green fiber with high-costs and a high performance. Compared with other fibers, basalt's overall performance is better, and it also meets the requirements for materials in the field of road engineering. Therefore, in recent years, increasingly more basalt fiber products have been applied in road engineering.

Shu Li [8], from the Ocean University of China added basalt fibers with a certain fiber length and content to cement-stabilized crushed stone. A series of mechanical and

durability tests showed that adding basalt fibers improved the compressive and splitting strength of cement-stabilized crushed stone, reduced its dry shrinkage and temperature shrinkage coefficient, and improved its anti-shrinkage performance. Yingbo Bao [9] added basalt fibers to cement-stabilized crushed stone to improve its crack resistance. According to their experiments, this addition reduced the dry shrinkage coefficient by 11% and the temperature shrinkage coefficient by 15%. Ming Yang [10] mixed a certain proportion of basalt fiber and polypropylene fiber into a cement-stabilized gravel base to explore the influence of hybrid fibers on pavement performance. Qiyi Wu et al. [11] employed a splitting test for a 7-day-old mixture, which showed that short basalt fibers significantly enhanced the splitting strength of cement-stabilized porous basalt gravel, with 18 mm fibers being enhanced due to the presence of 12 mm and 24 mm fibers. Therefore, the addition of basalt fibers can significantly improve the crack resistance of cement-stabilized crushed stone.

Haibo Hu [12] of Chang 'an University mixed basalt fiber strips of a certain width into cement-stabilized gravel, and conducted mechanical and durability tests. The results showed that the addition of basalt fiber strips of different widths reduced the compressive strength of the cement-stabilized gravel to a certain extent, but its anti-shrinkage performance was improved. The study demonstrated the strengthening effect of basalt-strip-reinforced cement-stabilized crushed stone.

Kun Yang [13] concluded that basalt fiber geogrid paving could extend the fatigue life of pavement structures and reduce project costs. Chuanli Deng et al. [14] added basalt fiber geogrids to rubble walls to study their influence on the compressive properties. The results showed that the maximum bearing capacity of the rubble walls was greatly improved and could even reach 1.6 times that of an ordinary rubble wall. Xiaokang Yang [15] set glass fiber gratings on top of the middle surface layer, lower layer, and base layer of a test section and collected bending, vertical tensile, and shear stress monitoring data for the road surface before and after laying, concluding that setting glass fiber gratings on top of the middle surface layer had the best preventative effect on reflection cracks. Xiaobin Wu [16] concluded that basalt fiber geogrids have certain positive effects on the reinforcement of roadbeds and pavement and that such materials are worthy of popularization and application. Yunpeng Li et al. [5] simulated the effect of the addition of basalt fiber nets to a slope under working conditions, and the results showed that the addition enhanced the stability of the slope and that the safety factor would be higher with a steeper slope within a certain range. Minghao Jia et al. [17] added basalt fiber geogrids and chopped basalt fiber to a cement matrix, respectively, to explore their effects on the compressive and flexural strength of the matrix. The results showed that both basalt fiber materials improved the mechanical properties and compressive and flexural strength of the cement matrix, but basalt fiber geogrids performed better. Wujie Ni et al. [18] used basalt fiber geogrids to stiffen a cement-stabilized gravel base. The geogrids were laid on top of the base and between the upper and the lower base, without basalt fiber grilles, and temperature and strain data were collected to analyze the influence of the different layers on the temperature shrinkage strain under the same test conditions. The results showed that the reinforcement effect of the basalt fiber geogrid layer between the upper and lower base was the best.

In conclusion, basalt fiber geogrids have a high fracture strength, low elongation, good physical and chemical stability, etc. They have a certain positive effect on subgrade and pavement engineering, slope protection, and masonry structure reinforcement. However, their application in engineering is still at the exploratory stage. As mentioned, Wujie Ni et al. [18] used basalt fiber geogrids to stiffen a cement-stabilized gravel base and determined that the best effect was to be found between the upper and lower base. However, they only compared the stiffening effect of basalt fiber geogrids between different levels on a trial road section and did not conduct systematic research indoors. In this paper, basalt fiber geogrids are laid between the base and the lower base of asphalt pavement, and their influence on the mechanical properties of cement-stabilized gravel is studied. This research has important social and economic effects in reducing the degradation of cement-stabilized

gravel bases, ensuring road service life and maximizing traffic capacity, saving maintenance funds, etc.

2. Materials and Methods

2.1. Test Materials

2.1.1. Basalt Fiber Geogrids

The selected geogrid material should have a high tensile strength and low elongation to meet the application requirements [19]. Basalt fiber macadam has excellent mechanical properties compared to all the kinds of geogrids on the market formed by high-molecular polymers, such as glass fiber, carbon fiber, and aramid. The maximum tensile strength of basalt fiber can be as high as 5000 MPa, which is higher than that of geosynthetic materials made of general fibers, and its elongation at break is less than 3%, with a higher erosion resistance than that of other fiber products. Therefore, the EGA100-100 kN basalt fiber geogrids produced by Feicheng Lianyi Engineering Plastics Co., LTD., Feicheng, China was selected in this study. Their performance is shown in Tables 1 and 2.

Table 1. Physical parameters of the geogrids.

Parameter Index	Mean Value (*n*)	Standard Deviation (σ)	Coefficient of Variation (Cv)	Final Value
Mass per Unit Area (g/m^2)	596.67	20.83	3.5	596.67
Mesh Size (mm)	4.8	0.929	2.03	4.8
Width (m)	5.45	0.836	1.38	5.45
Grid Shape		Rectangle		

Table 2. Mechanical parameters of the geogrids.

Property	Unit	Transverse Direction		Longitudinal Direction	
		Standard Value	Test Value	Standard Value	Test Value
Center Distance of Mesh	mm	---	50.8	---	50.8
Breaking Strength	kN/m	100	≥102.2	100	≥103.9
Elongation at Break	%	≤3	2.7	≤3	2.8

2.1.2. Cement

As a material that can be hardened both in air and water, cement is different from other air-hardening cementing materials in that it can maintain its strength continuously and even further develop its strength after hardening in water [20]. Early-strength cement and fast-hardening cement are not suitable as base materials, and ordinary Portland cement, slag Portland cement, and volcanic Portland cement are usually used as semi-rigid base materials. In general, grade 32.5 or 42.5 cement is used as a binding material. The cement used in this test is P.O 42.5 ordinary Portland cement, and its technical parameters are shown in Table 3.

Table 3. Cement-related technical parameters.

Item	Flexural Strength (MPa)		Compressive Strength (MPa)		Setting Time		Water Requirement for Cement Standard Consistency (%)	Cement Soundness	Fineness (%)
					min	h			
	3 d	28 d	3 d	28 d	Initial Setting Time	Final Setting Time			
Specification Value	≥3.5	≥6.5	≥16	≥42.5	≥45	≤10	≤30	Qualified	≤10
Test Value	4.5	7.6	25.2	48.2	98	7	28.6	Qualified	6.8
Conclusion	The cement meets the specification requirements and is a qualified cement								

2.1.3. Aggregate

For semi-rigid base materials, the maximum particle size of the aggregate must be limited to ensure the suitability of the base material construction. For high-grade asphalt

pavements, aggregates with a smaller maximum particle size must be used because of the higher requirements for structural layers and road smoothness. According to the relevant specifications, the maximum particle size of aggregates in China's high-grade asphalt pavement bases should not exceed 31.5 mm.

2.1.4. Optimal Grading of Coarse and Fine Aggregate

The test results of the relevant aggregate are shown in Tables 4–6.

Table 4. Test results of the aggregate technical indexes.

Item	Crushing Value (%)	Apparent Density (g/cm^3)	Needle Flake Content (%)	Void Rate (%)	Liquid Limit (%)	Shrinkage Limit Index (%)
Specification Value	<30	>2.5	<20	<47		
Test Value	15	2.74	10.6	45.8	12	4
Conclusion	Aggregate technical indicators meet the specification requirements					

Table 5. Sieving results for each grade of the coarse aggregates (passing rate %).

Sieve Hole Size (mm)	31.5	26.5	19	16	9.5	4.75	<4.75
19–31.5 mm	100	76.3	14.2	2.8	0.8	0.8	0.8
9.5–19 mm	100	100	98.7	91.0	24.6	1.4	0.2
4.75–9.5 mm	100	100	100	100	99.4	17.2	4.5

Table 6. Sieving results for each grade of the fine aggregates (passing rate %).

Sieve Hole Size (mm)	4.75	2.36	1.18	0.6	0.075
0–4.75 mm	95.1	61.1	40.3	22.2	10.1

The test results of the coarse and fine aggregates meet the relevant technical specifications. According to the sieving results used in the base construction of the Yanchong Expressway, the grading composition of the coarse and fine aggregates used in this test is shown in Figure 1.

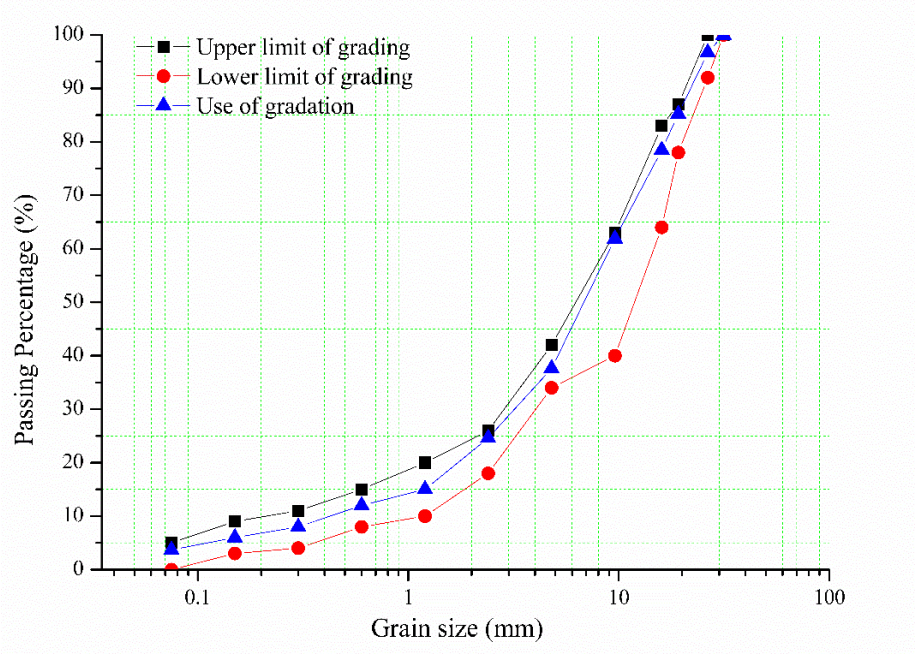

Figure 1. Aggregate grading curve.

2.2. Test Methods

2.2.1. The Compaction Test Method

The base mix ratio is determined by an indoor standard compaction test, and the test applies a construction-site mix ratio. The standard compaction test was performed according to T 0804-1994 in Chinese standard "Test Methods of Materials Stabilized with Inorganic Binders for Highway Engineering" (JTG E51-2009 [20]). The compaction test methods used in various countries are very similar and will not be described in detail here.

2.2.2. Specimen Preparation and Curing

Hydrostatic molding of the specimen was performed according to T 0844-2009 in Chinese standard JTG E51-2009. In this paper, static pressing is adopted. With this method, the specimen is pressed at the upper and lower part of the die to compact the mixed material. In the process of specimen forming, the mixture is added to the mold twice; in the first occasion, half of the mass of the mixture is added. After ramming via a ramming rod, the basalt fiber geogrids are added to the mold, and then the other half of the mixture is added to be compacted by the press. The size of specimens for the unconfined compressive strength test, splitting strength test, and compressive resilience modulus test was φ150 mm × 150 mm, and the size of specimens for the flexural tensile strength test was 100 mm × 100 mm × 400 mm.

The specimens were all placed in a standard curing box at approximately 20 °C with a humidity higher than 95% for curing. Unconfined compressive strength, splitting strength, compressive resilience modulus, and flexural tensile strength were measured at different ages of 7 days, 28 days, and 90 days, respectively. All the tests were divided into two groups: PT-3.8 without geogrids and BG-3.8 with basalt geogrids. The maximum aggregate particle size was 26.5 mm. In order to ensure the reliability and accuracy of the test results, the number of cylindrical specimens in each group was 13, and the number of girder specimens in each group was 15. A total of 234 cylindrical specimens and 90 beam specimens were prepared.

2.2.3. Unconfined Compressive Strength Test

As an important index, the unconfined compressive strength of a specimen is used to judge whether the material meets the required pavement performance of the base.

In this test, sample preparation was performed according to T 0805-1994 in Chinese standard JTG E51-2009 [20]. The universal testing machine selected for this test has a maximum measuring range of 400 kN and a measuring accuracy of ±1%. It can be uniformly and continuously loaded and unloaded and can maintain a fixed load, with a loading rate that can be effectively controlled at 1 mm/min. During the gradual loading of the press, changes in its values can be observed, and the maximum pressure value can be recorded when the specimen is damaged.

The unconfined compressive strength of the specimen was calculated according to Formula (1).

$$R_c = \frac{P}{A} \tag{1}$$

In this formula:

R_c—the unconfined compressive strength (MPa);

P—the maximum pressure of the specimen (N);

A—the height of the specimen (mm^2).

In testing the same group of specimens, the outliers were removed by the 3× mean square error method, and test specimens had 2 to 3 outliers. A test was performed again if the number of outliers exceeded the above provisions. If the coefficient of variation (%) of a same group of tests was less than 15%, it was considered a valid test. If the C_v of the test results could not be guaranteed to be less than the specified value, the required number of specimens was should be recalculated according to the allowable error probability of 10%

and 90%, and the number of specimens was increased, and new tests were performed. The results of new and old tests were re-evaluated until the C_v met the requirements.

The allowable C_v is calculated according to Formula (2).

$$C_v = \frac{S}{\overline{x}} \tag{2}$$

In this formula:
C_v—the allowable coefficient of variation;
$\overline{x}$—the arithmetic mean;
S—the standard deviation.

$$S = \sqrt{\frac{1}{n-1}\sum_{i=1}^{n}(x_i - \overline{x})^2} \tag{3}$$

n is determined by Formula (4)

$$n = \left[t_{1-a/2}C_v|e|\right]^2 \tag{4}$$

In this formula:
n—the test quantity;
$t_{1-a/2}$—the quantile values in the T-distribution table;
$|e|$—the allowable error is 10% here.

2.2.4. The Test Method for Splitting Strength

Generally, splitting strength measured by a splitting test (also called an indirect tensile test) is used to evaluate the ability of semi-rigid materials to resist tension (Chinese standard JTG/TF20-2015 [21]).

The splitting strength test was performed according to T 0806-1994 in Chinese standard JTG E51-2009 [20]. The instrument used in this test is a universal testing machine. A batten is placed on the lifting platform of the press, the specimen is placed on the batten horizontally, and a batten is placed on the top surface of the specimen (the contact line between the upper and lower batten and the specimen must be located at both ends of the diameter of the specimen and perpendicular to the lifting platform). A spherical support is placed on the upper batten and located at the middle of the specimen. During the test, deformation should be increased at the same speed, and the loading rate should be maintained at 1 mm/min, recording the maximum pressure when the specimen is broken. The indirect tensile strength of the specimen was calculated according to Formula (5) or (6).

When the loading batten is not set:

$$R_i = \frac{2P}{\pi dH} \tag{5}$$

In this formula:
R_i—the splitting strength of the specimen (MPa);
P—the maximum destructive power of the specimen (N);
H—the height of the specimen (mm);
d—diameter of the specimen (mm).
When setting up the loading batten:

$$R_i = \frac{2P}{\pi aH}\left(sin2\alpha - \frac{a}{d}\right) \tag{6}$$

In this formula:
a—width of layering section (mm);
α—the center angle corresponding to the width of the half-layering strip.
The other symbols have the same meaning as above.

The treatment method of the test results is the same as that of the unconfined compressive strength test.

2.2.4.1. The Test Method for Modulus of Compressive Resilience

The compressive resilience modulus test was performed according to T 0807-1994 in Chinese standard JTG E51-2009 [20]. The previous universal testing machine was used in this test, the measurement accuracy was ±1%, and the loading rate could be effectively controlled at 1 mm/min. A round metal plane-loading top plate and round metal plane loading bottom plate were used: the diameter of the plates should be greater than the diameter of the test piece and the bottom plate diameter line both sides of the column, which is equipped with a dial gauge clip.

After the specimen was soaked in water for 24 h prior to test, it was dried and placed on the loading base plate. A small amount of 0.25~0.5 mm fine sand was sprinkled on the top surface of the specimen, and the loading plate was manually pressed and rotated fill any microscopic surface irregularities with the find sand and disperse excess. This increases the contact area between the roof and the specimen.

Preloading: The preloading and unloading test was carried out twice with half of the maximum load applied, so that the loading roof was in close contact with the surface of the specimen. After waiting 1 min after every two unloads, the short pointer of the dial gauge was set to the middle position and the long pointer was set to 0 to record the original reading of the dial gauge.

Rebound deformation measurement: The predetermined unit pressure was divided into 5~6 equal parts as the pressure value to be applied each time. The actual load applied was one step higher than the predetermined level. After the first-level load was applied for 1 min, the reading of the dial meter was recorded, and the load was removed at the same time, so that the elastic deformation of the specimen was restored. After recording the reading of the dial meter at 0.5 min, the second-level load was applied the same as before. After waiting 1 min the reading of the dial meter was recorded, and the load was removed. At 0.5 min after unloading, the reading of the dial gauge was recorded, and the third-level load was applied. This was performed step by step until the rebound deformation under the last stage of loading was recorded.

The elastic deformation l under each stage of loading is calculated according to Formula (7).

$$l = Pressurized\ reading - Depressurization\ reading \quad (7)$$

With unit pressure p as the horizontal coordinate (to the right) and rebound deformation l as the longitudinal coordinate (down), the relationship curve between p and l is drawn, and the false deformation at the beginning of the curve is corrected. When correcting, under normal circumstances, the first and second test points are taken as a straight line, and the line is extended to intersect the vertical axis, and the intersection point is the new origin.

The resilience modulus is calculated according to Formula (8)

$$E_C = \frac{Ph}{l} \quad (8)$$

In the formula:
E_C—compressive resilience modulus (MPa);
P—unit pressure (MPa);
h—specimen height (mm);
l—rebound deformation of the specimen (mm)
The treatment method of test results is the same as that of unconfined compressive strength.

2.2.4.2. The Test Method for Flexural Tensile Strength

The flexural tensile strength test was performed according to T 0851-2009 in Chinese standard JTG E51-2009. The test was carried out using a three-point pressure method, and

the three-point position was marked on the side of the specimen (parallel to the direction of pressure when the specimen was formed). The specimen was placed on the test rack, with the load direction being consistent with the pressure direction when the specimen was formed, and the upper and lower pressing blocks were located at the three-point position of the specimen. According to the test requirements, a displacement sensor was placed in the beam span to measure the mid-span displacement under the ultimate load. The loading rate was 50 mm/min until the specimen was damaged, and the failure limit load was recorded. Then, the flexural tensile strength was calculated according to Formula (9).

$$R_S = \frac{PL}{b^2 h} \tag{9}$$

In this formula:
R_S—flexural tensile strength (MPa);
P—failure limit load (N);
L—span, that is, the distance between the two fulcrums (mm);
b—specimen width (mm);
h—specimen height (mm).

3. Results and Discussion

3.1. The Compaction Test

The compaction test curve is drawn with the moisture content of the compacted sample as the horizontal coordinate and the corresponding dry density as the longitudinal coordinate. The vertical coordinate of the curve apex is the maximum dry density of the water-stable material, and the horizontal coordinate is the highest moisture content, as shown in Figure 2.

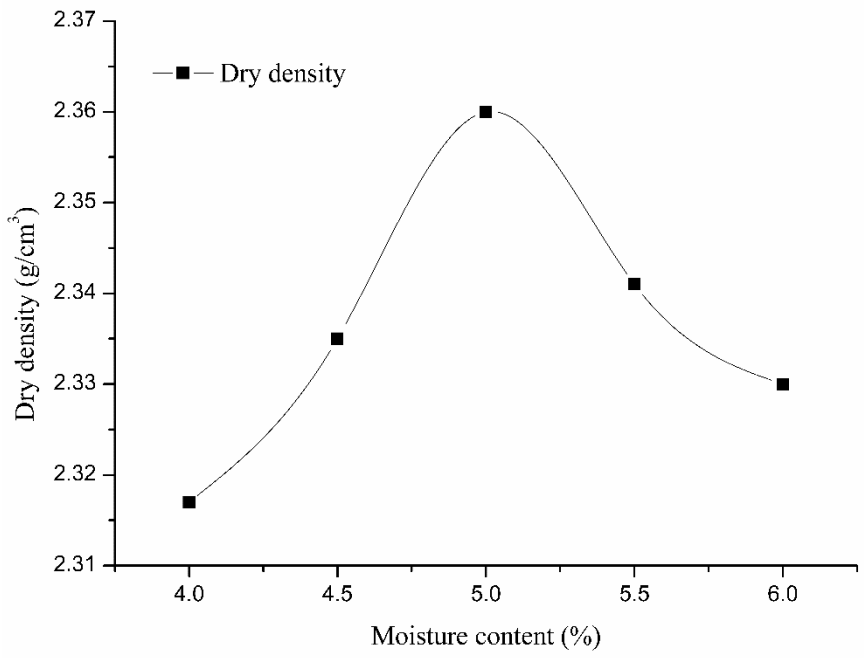

Figure 2. Laboratory standard compaction test curve.

Based on the above test results, it can be concluded that the best water content of cement-stabilized gravel is 5.0%, the maximum dry density is 2.361 g/cm^3, and the cement dose is 3.8% (referring to the actual construction amount at the site).

3.2. Unconfined Compressive Strength Test Results and Analysis

Based on the unconfined compressive strength test data, the unconfined compressive strength of the two groups of cement-stabilized macadam increases with age (as shown in Figure 3).

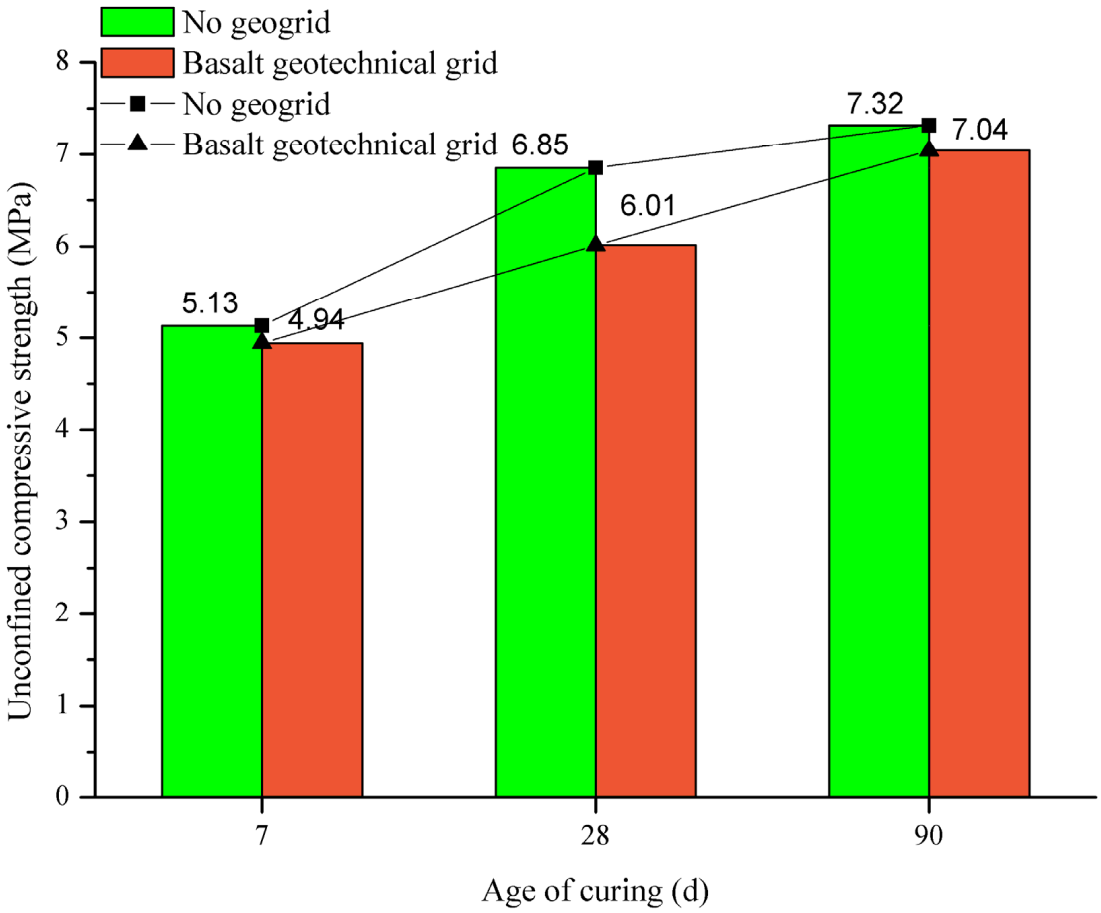

Figure 3. Variation in unconfined compressive strength with curing age.

The strength of cement-stabilized crushed stone is affected by many factors, such as mixture grading, the dosage of cement, water content, and maximum dry density, but is mainly affected by the hydration of the cement, together with other factors such as ion exchange and chemical stimulation. However, from the unconfined compressive strength test results, it can be seen that the compressive strength of cement-stabilized crushed stone with the addition of basalt geogrids is slightly lower than that of ordinary cement-stabilized crushed stone at different ages. After 28 days, the strength gap between the two reaches its greatest degree, and the compressive strength of ordinary cement-stabilized crushed stone is 14% higher than that stabilized by the basalt fiber geogrids. However, after 90 days, the compressive strength of the two is similar. It can be seen that the addition of basalt fiber geogrids reduces the integrity of cement-stabilized gravel to a certain extent, resulting in an early-strength formation that is hindered by the geogrids, but in the process of increasing strength, this shortcoming gradually weakens. This is because the unconfined compressive strength of the specimen is mainly determined by the bearing capacity of the aggregate structure of the cement-stabilized gravel, and the formation of the bearing capacity of the aggregate structure will be affected by the laying of the basalt fiber geogrids. However, there is little difference between the two when the compressive strength is completely formed after 90 days. In the process of unconfined compression, there will be a certain tensile effect, and the addition of basalt fiber geogrids improves the tensile capacity of the cement-stabilized gravel, thus improving part of the compressive capacity.

3.3. Splitting Strength Test Results and Analysis

According to the test data and the results calculated by Formulas (1) and (2), the relationship between the splitting strength and curing age was drawn (as shown in Figure 4).

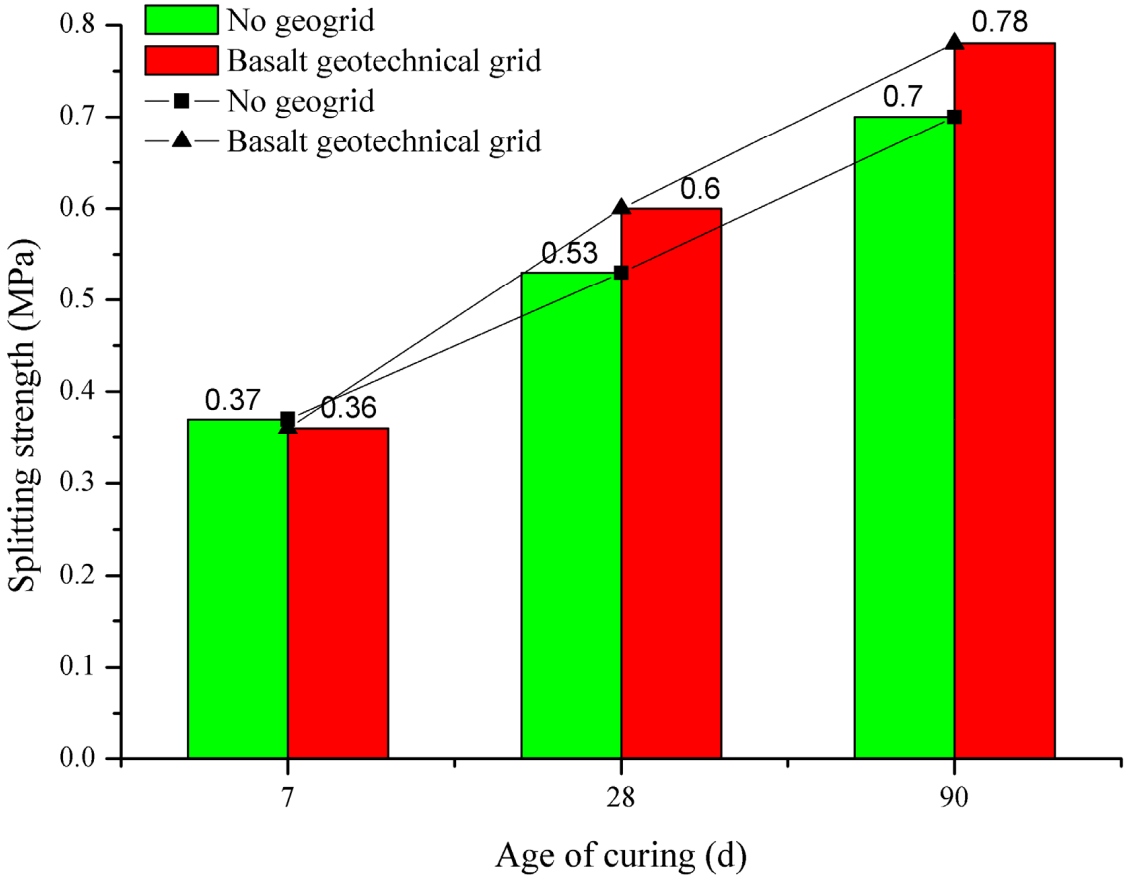

Figure 4. Variation in splitting strength with curing age.

It can be seen from Figure 4 that with an increase in age, the splitting strength of BG-3.8 and PT-3.8 specimens also increases continuously, and the splitting strength of the specimens with basalt fiber geogrid reinforcement increases to some extent. When the curing age reaches 7 d, 28 d, and 90 d, the average unconfined compressive strength of BG-3.8 specimens is 0.36 MPa, 0.6 MPa, and 0.78 MPa, while the average splitting strength of PT-3.8 specimens is 0.37 MPa, 0.53 MPa and 0.7 MPa, respectively. The splitting strength of reinforced specimens is −2.7%, 13.2% and 11.4% higher than that of unreinforced specimens, respectively.

At the beginning of curing, there was little difference in the splitting strength between BG-3.8 and PT-3.8 specimens. It can be considered that in the initial stage of specimen strength formation, the bonding action of the cement-stabilized gravel base is weak, and the integrity of the basalt fiber geogrid and cement-stabilized gravel base is poor. In the late curing period, the cement-stabilized gravel exhibits a good bonding effect. At this time, the cement-stabilized gravel and geogrids jointly play a stretching role. The geogrids enhance the tensile strength of the cement-stabilized gravel base, and the splitting strength also increases. This is consistent with the research results of Xiaopeng Yang [22].

3.4. Compressive Resilience Modulus Test Results and Analysis

According to the test data and the calculation results of Formula (8), the relationship between compressive resilience modulus and curing age was drawn (as shown in Figure 5).

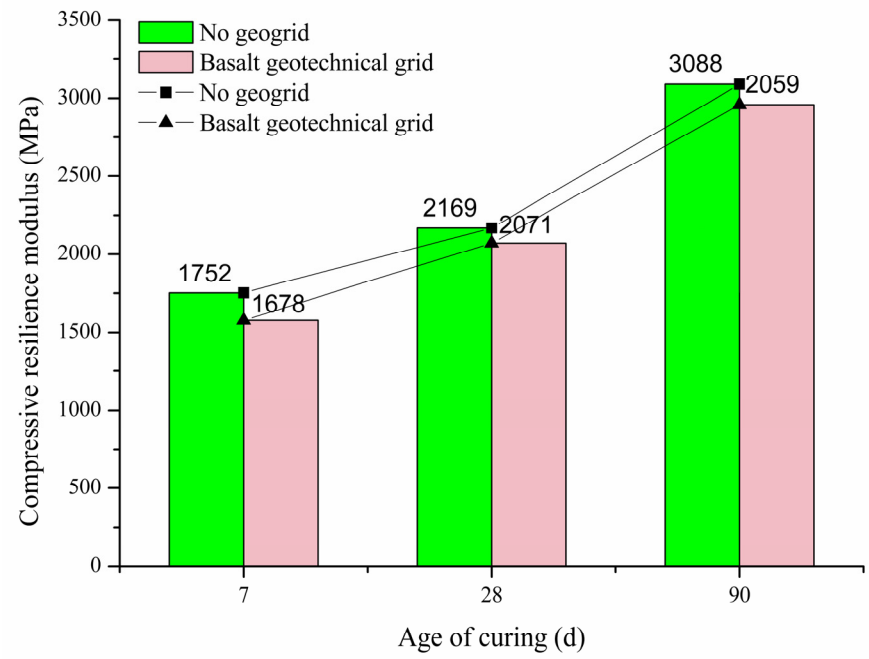

Figure 5. Variation in compressive rebound modulus with curing age.

It can be seen from Figure 5 that the compressive resilience modulus of the two specimens increases with age, while the compressive resilience modulus of the specimens with basalt fiber grating decreases slightly. When the curing age reaches 7, 28, and 90 d, the average compressive modulus of BG-3.8 specimens is 1678, 2071, and 2959 MPa, respectively, while the average compressive modulus of PT-3.8 specimens is 1752, 2169, and 3088 MPa, respectively. The compressive resilience modulus of the reinforced specimens decreased by 4.2%, 4.5%, and 4.1% compared to the unreinforced specimens.

The compressive resilience modulus of BG-3.8 specimens is always slightly lower than that of PT-3.8 because the modulus of basalt fiber grating is low. After adding cement-stabilized gravel material, the deformation resistance of water-stabilized gravel is reduced, but the reduction is small, which is equivalent to reducing the stiffness of the material, thus effectively improving the toughness of the base, which is consistent with the conclusion of some scholars [23].

3.5. Flexural Tensile Strength Test Results and Analysis

According to the relevant data, the relationship between the flexural and tensile strengths of the two groups of cement-stabilized gravel and its curing age was drawn (Figure 6).

As shown, the flexural and tensile strength of the two specimens increased with age, and was significantly improved after basalt fiber grille reinforcement. When the curing age reached 7, 28, and 90 days, the average flexural tensile strength of BG-3.8 specimen was 0.52, 0.79 and 1.28 MPa, respectively, while the average flexural tensile strength of PT-3.8 specimens was 0.43, 0.63, and 1.00 MPa, respectively. The flexural tensile strength of the reinforced specimens was 20.9%, 25.3%, and 28% higher than that of the unreinforced specimens. The increase in the flexural tensile strength of specimens of different ages after reinforcement was higher than 20%, and it increased with an increase in age.

The reason is that the addition of basalt fiber geogrids has a tensile effect, improving the bending and tensile resistance of the base structure. With an increase in curing age, the integrity of the geogrid and water-stabilized gravel base is continuously improved, and the flexural tensile strength is also increased.

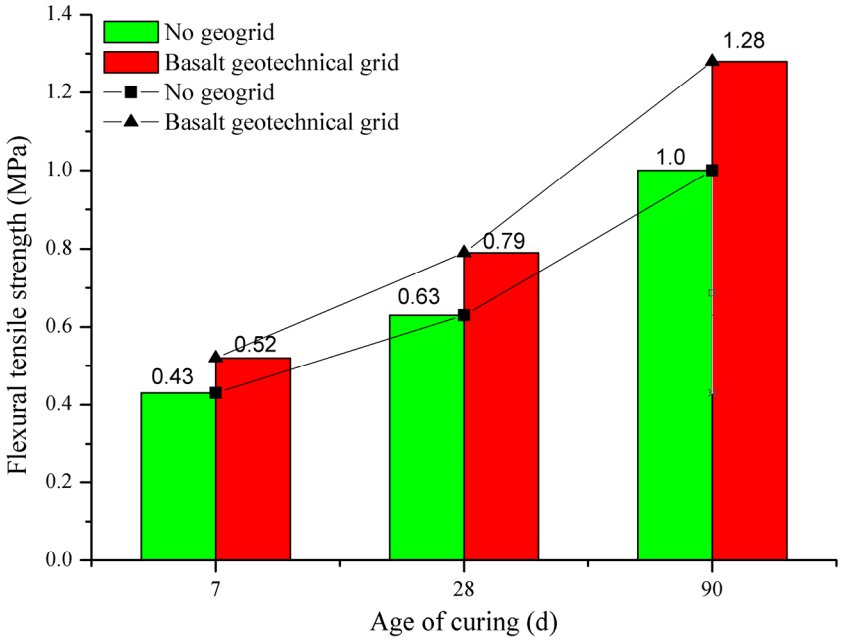

Figure 6. Variation in flexural tensile strength with curing age.

The addition of basalt fiber geogrids to cement-stabilized gravel is equivalent to adding rebar to cement concrete, which plays a certain tensile role, thus delaying the bending and tensile failure of cement-stabilized gravel to a certain extent. In the early stage of curing, the strength of cement-stabilized crushed stone has not fully formed, so the flexural and tensile strengths are higher than that of ordinary cement-stabilized crushed stone. During the flexural tensile strength tests, there were cracks above and below the basalt fiber geogrid cement-stabilized gravel specimens, but due to the existence of the geogrids, the entire specimens did not exhibit completely cracked surfaces. With increasing curing age, the cement-stabilized gravel and geogrids formed an organic whole. At this time, the flexural tensile strength of the basalt-fiber-geogrid-stabilized gravel gradually reached its maximum value, and the difference between the two gravels became the largest.

4. Conclusions

This paper conducted a comparative study on the unconfined compressive strength, splitting strength, compressive resilience modulus, and flexural tensile strength of basalt fiber-geogrid-reinforced and ordinary cement-stabilized gravel specimens at three ages (7 days, 28 days, and 90 days). The conclusions of the research are as follows:

(1) The integrity of the base structure is reduced after the reinforcing the basalt fiber geogrids. The compressive strength of the water-stabilized gravel base decreases in the early stages, but gradually increases until a curing age of 90 days. The strength of the base meets the design requirements.

(2) With an increase in curing age, the splitting strength of basalt-fiber-geogrid-reinforced specimens is greatly increased due to the continuous enhancement of the bonding effect of the basalt fiber geogrids within the base. The basalt fiber geogrids utilize their full tensile capacity and improve in strength.

(3) The compressive resilience modulus of the water-stabilized gravel base decreased by about 4.5% after reinforcement, indicating that reinforcing basalt fiber geogrids had little effect on the overall compressive capacity of the base.

(4) After reinforcement, the flexural tensile strength of the water-stabilized gravel base increased by more than 20%, which is due to the addition of the geogrids enhancing the tensile and flexural strength of the base.

(5) The basalt fiber grids were laid in the middle of the cement-stabilized gravel base, and the mechanical properties were improved as a whole. This approach can be applied to

actual projects, even though it increases the challenges and difficulty of constructing the base. However, if supporting machinery can be developed, the construction efficiency can be improved in the future.

Author Contributions: Conceptualization, Y.Z. and Y.H.; methodology, Y.Z., Y.H. and X.Y.; validation, Y.Z. and X.Y.; formal analysis, Y.H. and J.G.; investigation, Z.W.; data curation, Y.H.; Writing—original draft preparation, J.G., Y.H. and Z.W.; Writing—review editing, Y.H., Y.Z. and J.G.; visualization, J.G. and Y.H.; supervision, J.G. All authors have read and agreed to the published version of the manuscript.

Funding: This research is a part of the research project on crack resistance of semi-rigid base. The project (No. 220221200407) received a grant of 700,000 RMB from Hebei Provincial Department of Transportation.

Institutional Review Board Statement: Not applicable.

Informed Consent Statement: Not applicable.

Data Availability Statement: Data are contained within the article.

Conflicts of Interest: Authors Yu Zhu and Xiaodong Yuan were employed by the company Hebei Expressway Group Co., Ltd. The remaining authors declare that the research was conducted in the absence of any commercial or financial relationships that could be construed as a potential conflict of interest.

References

1. Wang, X.G. Causes and typical treatment methods of reflection cracks in semi-rigid base. *North. Commun.* **2019**, 44–46. [CrossRef]
2. Pan, R. Mechanical analysis of stress absorption layer of warm mixed rubber asphalt mixture to prevent reflection crack in cold area. *Highway* **2019**, *64*, 52–58.
3. Krystyna, K.F. Influence of Cracks on the Lifetime of Semi-Rigid Pavements. *Arch. Hydro-Eng. Environ. Mech.* **2016**, *63*, 83–100.
4. Tan, L.; Xiang, Y.G. Experimental study of glass fiber geoglass in the prevention of reflective cracks in asphalt pavement. *Highway* **2016**, *61*, 3–57.
5. Li, Y.P.; Chen, X.P. Application Evaluation of Basalt Fiber Net in Highway Slop Stability. *Highway* **2020**, *65*, 65–69.
6. Yang, J.; Chen, B.; Nuti, C. Influence of steel fiber on compressive properties of ultra-high performance fiber reinforced concrete. *Constr. Build. Mater.* **2021**, *302*, 124104. [CrossRef]
7. Zhang, D.; Tan, K.H.; Dasari, A.; Weng, Y. Effect of natural fibers on thermal spalling resistance of ultra-high performance concrete. *Cem. Concr. Compos.* **2020**, *109*, 103512. [CrossRef]
8. Li, S. Experimental Study on Pavement Performance of Basalt Fiber Cement Stabilized Macadam. Master's Thesis, Ocean University of China, Qingdao, China, 2014.
9. Bao, Y.B. *Performance Study of the Cement Stabilized Macadam with Basalt Fiber*; Chang'an University: Xi'an, China, 2017.
10. Yang, M. *Study on the Road Performance of Basalt–Polypropylene Hybrid Cement Stabilized Gravel*; Chang'an University: Xi'an, China, 2017.
11. Wu, Q.; Yao, H.; Hu, H. Effect of Basalt Fiber on Mechanical Properties of Cement Stabilized Porous Basalt Macadam. *Bull. Chin. Ceram. Soc.* **2022**, *41*, 192–198.
12. Hu, H.B. *Experimental Study on Crack Resistance of Reinforced Cement Stabilized Macadam Base by Basalt Fiber Belt*; Chang'an University: Xi'an, China, 2019.
13. Yang, K. Application of Basalt Fiber Geogrids in Bituminous Pavement. *Shandong Text. Econ.* **2015**, *215*, 18–19.
14. Deng, C.L.; Liu, X.; Fu, L. Experimental study on the compressive properties of Tibetan rubble wall with basalt fiber geogrid. *Sichuan Build. Sci.* **2017**, *43*, 5–8.
15. Yang, X. Analysis of mechanism and mechanical response of glass fiber grating to prevent reflective cracks in asphalt pavement. *Traffic World* **2020**, *23*, 27–28+31.
16. Wu, X. Research Progress on Application of Basalt Fiber in Civil Engineering. *Bull. Chin. Ceram. Soc.* **2020**, *39*, 1043–1049.
17. Jia, M.H.; Xiao, X.; Gu, Y. Comparative study on mechanical property of fiber and its grille reinforced cement matrix composite. *New Chem. Mater.* **2020**, *48*, 246–249.
18. Ni, W.; Shao, J.; Li, W.; Huang, Y.; Wang, J. Temperature shrinkage strain analysis of basalt fiber grid reinforced cement stabilized crushed stone base. *Adhesion* **2023**, *50*, 65–69.
19. *JT/T 776.3-2010*; Highway Science Research Institute, Ministry of Transport. Basalt Fiber and Product for Highway Engineering-Part 3: Basalt Fiber Geogrid. People's Communications Press: Beijing, China, 2010.
20. *JTG E51-2009*; Highway Science Research Institute, Ministry of Transport. Test Methods of Materials Stabilized with Inorganic Binders for Highway Engineering. China Communication Press: Beijing, China, 2009.
21. *JTG/T F20-2015*; Highway Science Research Institute, Ministry of Transport. Technical Guidelines for Construction of Highway Roadbases. China Communication Press: Beijing, China, 2015.

22. Yang, X.P. Study on mechanical properties of basalt fiber geoglyph reinforced water-stabilized gravel base. *Transp. World* **2023**, 60–62+83. [CrossRef]
23. Cheng, P.F. Research on Application Technology of Cement Stabilized Macadam Mixed with Basalt Fiber. Master's Thesis, Northeast Forestry University, Harbin, China, 2021.